ISSN: 2573-9565

Case Report

Journal of Clinical Review & Case Reports

Aloe vera gel conjugated cuttlefish bone graft material treated with three types of hydroxyapatite for clinical trial

Dong-Myong Kim[1*], Hyung-Kon Lee[1], Yong-Seong Kwon[1], Yeon-Mea Choi[2]

[1]*R&D Center, KJMBIO Ltd., 17 Saimdang-ro, Seocho-gu, Seoul, 06649, Korea.*

[2]*KimJeongMoon Aloe Ltd., 15 Saimdang-ro, Seocho-gu, Seoul, 06649, Korea.*

[*]Corresponding author
Dong-Myong Kim, R&D Center of KJMBIO Ltd., 17 Saimdang-ro, Seocho-gu, Seoul, 06649, Korea.

Submitted: 18 Mar 2022; **Accepted**: 26 Mar 2022; **Published**: 05 Apr 2022

Citation: *Dong-Myong Kim, Hyung-Kon Lee, Yong-Seong Kwon, Yeon-Mea Choi (2022) Aloe vera gel conjugated cuttlefish bone graft material treated with three types of hydroxyapatite for clinical trial. Journal of Clinical Review & Case Reports 7(4):68-76.*

Abstract

We have developed three types of hydroxyapatite particle (HP) functionalized Aloe vera gel W (AGW®) conjugated cuttlefish bone graft materials (Aloe-CGMs) for clinical applications. These Aloe-CGMs were prepared by attaching platelet, needle, and sphere shaped HPs to the surface of cuttlefish bone graft materials through chemically AGW® conjugation. Although all three HPs contributed to increase the surface area of graft material (GM), the shape of the HPs was a determining factor. Platelet HPs were most effective, because they caused a 62.3% increase in GM surface area whereas the influence of the spherical particle was only a 5.2% increase. This suggests that geometric factors regarding both the attached HPs and graft material surface are essential in controlling the surface roughness of graft materials. Among the three HPs, it was the platelet HPs that helped to increase the efficacy of the GM most significantly. Compared with GM with no HP attachment, Aloe-CGMs with platelet shaped HP (platelet Aloe-CGMs) treatment had ~58.9% higher cell attachment and proliferation rate. The MTT assay also showed that the HP treated cuttlefish bone graft materials had negligible cytotoxicity.

Keywords: *Aloe vera* Gel, Conjugation Method, Cuttlefish Bone, Graft Material, Hydroxyapatite, Bone Graft.

Introduction

Bone grafting is a surgical operation carried out to physically replenish a missing or weak bone and stimulate the growth of the osteoblasts on it [1]. For efficient bone grafting, a suitable scaffold is required. For example, graft materials (GMs) should have structures similar to those of bones, with a large specific surface area and high porosity [2,3], to stimulate the growth of osteoblasts. They should also cause low immune responses and low risks of infection to minimize danger in clinical use.

GMs can be classified as autografts, allografts, xenografts, and alloplastic grafts, based on the origin of the materials [4]. Because autologous graft materials are from the patient's own body, they are ideal graft materials, with high osteogenesis, osteoinduction, and osteoconduction. However, it is generally expensive and painful to use autografts because an additional surgery is needed to obtain them from the patient's body. Allografts, obtained from individuals who are not treated with the graft, can be an alternative choice but they are also expensive and there may be concerns about infection and immune response. Alloplastic grafts are synthetic materials, so they are relatively cheap. However, because the mechanical and structural properties of alloplastic grafts are very different from natural bones, their performance is generally not as good as other graft materials [5]. However, xenografts have many advantages over other graft materials [6]. Being prepared from animal bones, xenografts have major components and micro and nanoscale structures similar to human bones [7]. Having high osteoinduction and osteoconduction, xenografts provide a good environment for osteoblasts to attach and proliferate [8]. Furthermore, the degree of immune response occurring with xenografts has been reported to be smaller than with allografts [9]. Additionally, because xenografts are collected from animals, they can be obtained in larger quantities at much cheaper prices than autografts or allografts.

Because of these important advantages, xenografts have been well studied and some are available commercially [10]. Bovine bones are one of the most frequently used materials as xenografts, but they now have the potential risk of mad cow disease. To bypass this problem, we developed a xenograft material obtained from cuttlefish bone [11]. Being similar to human organs and tissues with less concern about human health issues, cuttlefish bone based materials have potential to serve as an excellent choice with improved biological and mechanical efficacy.

It has been reported that the surface roughness of GM is a key

factor in stimulating osteoblast attachment and proliferation, neovascularization, promotion of periodontal tissue, and bone formation [12-14]. Thus, it may be possible to enhance the performance of xenografts by increasing their surface roughness. Processes such as heat treatment or etching are typically used in metallic or ceramic materials to increase their surface roughness [15]. However, these are not desirable for xenograft materials because heat treatment processes can disrupt micro and nano scale structures of bones while the chemicals used for etching can increase the toxicity of graft materials [16]. Thus, a new method applicable to increasing the surface roughness of xenograft materials is desirable.

Hydroxyapatite particles (HPs) are biocompatible materials [17-19] often used in orthopedics and dentistry [20] as substitutes for bones and teeth [21]. Because HPs are composed mainly of elements similar to bones and have large surface area to volume ratios [22], they are strong candidates to replace bones and teeth. HPs have been used with various polymers [22-30], ceramics [31], and metals [32-34] to make alloplastic materials [35-36] However, to our knowledge, there is no report applying HAp NPs to xenografts to change their surface properties and improve their performance.

This study purposes the development of Aloe vera gel W (AGW®) conjugated cuttlefish graft materials (Aloe-CGMs) for clinical applications. We exploited a chemically AGW® conjugation method to attach HPs with different shapes, such as platelets, needles, and spheres, to the surface of grafts prepared from cuttlefish bone to change their surface morphology and surface area. Then, we investigated whether the attached HPs could improve the biological activities of graft materials and whether there was any variation between particles of different shapes.

Materials and Methods

Materials

Most of the materials used for HP synthesis and surface functionalization, such as type B gelatin (from bovine skin), alendronate, succinic anhydride, 1-ethyl-3-(3-dimethylaminopropyl)carbodiimide hydrochloride (EDAC), s-NHS, MES and NaOH, were purchased from Sigma-Aldrich (St Louis, MO, USA). Ca(NO3)$4H_2O$, NaH_2PO_4•$2H_2O$ and urea were from Junsei Chemical Co, Ltd. (Tokyo, Japan). Na_2HPO_4 and NaH_2PO_4 were purchased from Samchun Chemical (Seoul, Korea). DMSO was purchased from Daejung Chemical (Siheung, Korea). *Aloe vera* gel W (AGW®) and Aloe-CGMs were from KimJeongMoon Aloe Ltd. (Jeju, Korea).

MC3T3-E1 cells used in this experiment were provided at the Lab of Biomedical Science, Jeju National University (Jeju, Korea). Alpha minimal essential medium (α-MEM) was purchased from Gibco (Carlsbad, CA, USA) and the Quant-iT PicoGreen dsDNA assay kit was purchased from Invitrogen (Carlsbad, CA, USA). 3-(4,5-dimethylthiazol-2-yl)-2,5-diphenyltetrazolium bromide (MTT) was purchased from Calbiochem (San Diego, CA, USA).

Synthesis of Hydroxyapatite Particles

We modified previously reported synthesis methods to prepare platelet, needle, and spherical shaped HPs [37,38]. Specifically, gelatin 500 mg, $Ca(NO_3)$•$4H_2O$ 2.41 g, NaH_2PO_4•$2H_2O$ 1.49 g, and urea 1.214 g were all dissolved together in 500 mL of water. A small amount of NaOH (0.1-2 M) was added to the mixed solution to adjust pH. To synthesize platelet HAp NPs, the pH of the solution was adjusted to 7.5 and the reaction was carried out at room temperature. The pH of the mixed solution was tuned to 10 and 13 for the synthesis of needle and sphere shaped HPs, respectively. The mixed solution was reacted at 90°C for 96 h to synthesize needle and sphere shaped HPs. A purification process was followed by centrifuging the synthesized particles at 4500 rcf for 10 min and replacing the supernatant with DI water (18 MΩ•cm). This process was repeated six times.

Preparation of Bone Graft Materials From Cuttlefish Bone

Raw cuttlefish bone was obtained from the National Institute of Fisheries Science (Jeju, Korea). A diamond saw was used to cut the large cuttlefish bone into small pieces (15×15 mm). To remove organic matter, the porcine pieces were stirred in 30% hydrogen peroxide for 12 h and 80% ethyl alcohol for 12 h. After rinsing with distilled water, bone pieces were dried for 24 h at 100°C and then heat treated at 600°C in an oxygen atmosphere box furnace to remove collagen and organics. Finally, the bone pieces were ground with a grinder.

Chemically AGW® Conjugation of HPs on the Cuttlefish Bone Graft Materials

For amine functionalization on HPs and GMs, the surface of HPs and GMs were both reacted with AGW® [39,40]. For the reaction, 30 mg of HPs or GMs were dissolved in 10 mL of water and 0.15 mg of AGW® was added afterwards. The mixed solution was reacted at 37°C for 12 h. After the reaction, the particles were purified by centrifuging the solution at 4500 rcf for 10 min and replacing the supernatant with 10 mL of DI water. This process was repeated six times. The GMs were centrifuged at 7 rcf for 1 min for the purification.

For carboxyl functionalization of GMs, subsequently, the amine modified GMs were functionalized with carboxyl groups [41]. For the functionalization, GMs were dissolved in 10 mL of phosphate buffer (pH 7.4, 0.1 M) and 0.46 mg of succinic anhydride was then added. The reaction was carried out at room temperature for 3 h with gentle shaking with digital rocker at 40 rpm. After the reaction, the GMs were centrifuged at 7 rcf for 1 min for purification and the supernatant was replaced with 10 mL of MES buffer (pH 5.0, 0.1 M). This process was repeated six times.

For the attachment of HPs on GMs for Aloe-CGMs formation, 0.88 mg of EDAC and 2.5 mg of s-NHS were added to MES buffer 3 mL (pH 5.0, 0.1 M) containing 30 mg of BGMs [41,42].

The mixture was shaken for 2 h at room temperature. After the reaction, amine-modified HPs were added to the solution containing EDAC and s-NHS-treated GMs for >2 h with gentle shaking. After the reaction, the GMs were centrifuged at 7 rcf for 1 min for purification and the supernatant was replaced with 10 mL of DI water. Because most HPs remained in the supernatant at 7 rcf, the unreacted particles could be removed from the GMs. This process was repeated six times.

Cell Culture and Assay

Cell culture of MC3T3-E1 : Prepared GMs (40 mg) with or without HP surface treatment were put in a 48-well cell culture plate. These samples were washed three times with ethanol and PBS solution (137 mM NaCl, 10 mM Na_2HPO_4). Then, the Aloe-CGMs were placed on a clean bench and irradiated with UV radiation overnight for sterilization. After UV irradiation, 1 mL of α MEM media containing FBS and antibiotics (penicillin/streptomycin) and 1×10^5 cells were placed in each well. The cell culture plate was incubated at 37°C in a 5% CO_2 incubator for 2 days [43].

After incubation, we removed the medium from the cell culture plate and washed the cells using PBS solution. These cells were detached from the plate by treating them with trypsin/EDTA solution for 3 min. We then added 700 µL of α MEM media to each cell suspension and mixed well. This cell suspension was transferred to a 1.5 mL centrifuge tube and centrifuged (1,500 rpm, 5 min). We removed the supernatant and dissolved the cell pellet in TE buffer (10 mM Tris-HCl, 1 mM EDTA, pH 7.5).

Quant-iT PicoGreen dsDNA assay: Each cell suspension, 100 µL, was mixed with 200 µL of lysis buffer and was incubated at 65°C for 10 min. Then, the mixed sample was sonicated for 1 min. After placing 100 µL of each sample into the well of a 96-well plate, 100 µL of 1:200 diluted Picogreen reagents were added to each sample. After 5 min, we measured the fluorescence intensity of samples using a microplate reader.

Cell viability test: We used the 3-(4,5-dimethylthiazol-2-yl)-2,5-diphenyltetrazolium bromide (MTT) assay for a cell viability test. MC3T3-E1 cells (5×104) were incubated with different graft materials for 1 day in a 24-well plate. After removing the culture medium, 0.5 mg/mL MTT containing medium was added to the cells for 3 h at 37°C. Cells were washed with PBS and insoluble products were dissolved in DMSO. Absorbance was measured at 540 nm using a microplate reader.

Characterization

To assess surface morphologies of the HPs, GM, and Aloe-CGMs, we used a JEOL JSM-7600F field emission scanning electron microscope (FE-SEM). For the Fourier transform infrared spectrometry (FT-IR) measurements, a Bruker TENSOR 27 spectrometer was used. The prepared samples were spread on thallium bromoiodide (KRS-5) optical crystals and dried before taking FT-IR measurements. For the zeta potential measurements, we used a Nano ZS90 system from Malvern Co. For the X-ray diffraction (XRD) characterization, a Smart Apex II diffractometer (Bruker) was used. The theta-2 theta method was used for the XRD characterization. BET analysis (ASAP 2000, Micromeritics, GA, USA) was carried out to measure surface area of GMs or Aloe-CGMs samples. For the characterization, 100 µg of each sample was prepared and dried for 12 h at 90°C in a vacuum oven before measurements. BET measurement was carried out by inserting N2 gas through the vacuum port and monitoring the gas adsorbed on the material surface.

Results and Discussion

Formation of HP Bone Graft Material Complex

Figure 1 shows the surface morphologies of a GM and the HPs used in this work. The average length and width of GMs were 1.18±0.62 mm and 0.61±0.15 mm, respectively. The GMs had many spherical grains existing on the surface, with a size of 81±37 nm. Although various morphologies of particles can be synthesized [38,44,45], we chose platelet shaped, needle shaped, and sphere shaped particles as the three model HPs for our study.

The platelet HPs were elliptical shaped; the lengths of the major and minor axes were 165±37 nm and 81±16 nm, respectively. The thickness of the platelet HPs was 18±3 nm. The length and width of the needle shaped particles were ~127±6 nm and ~19±3 nm, respectively. The sphere shaped HPs had an approximate size of 42±8 nm, similar to the grain size of the GMs. X-ray diffraction (XRD) patterns with major peaks appearing at 25.7°, 31.8°, 32.1°, 33.0°, and 34.0°confirmed that all the synthesized nanoparticles were hydroxyapatite ($Ca_{10}(PO_4)_6(OH)_2$) (Figure 1E) [37].

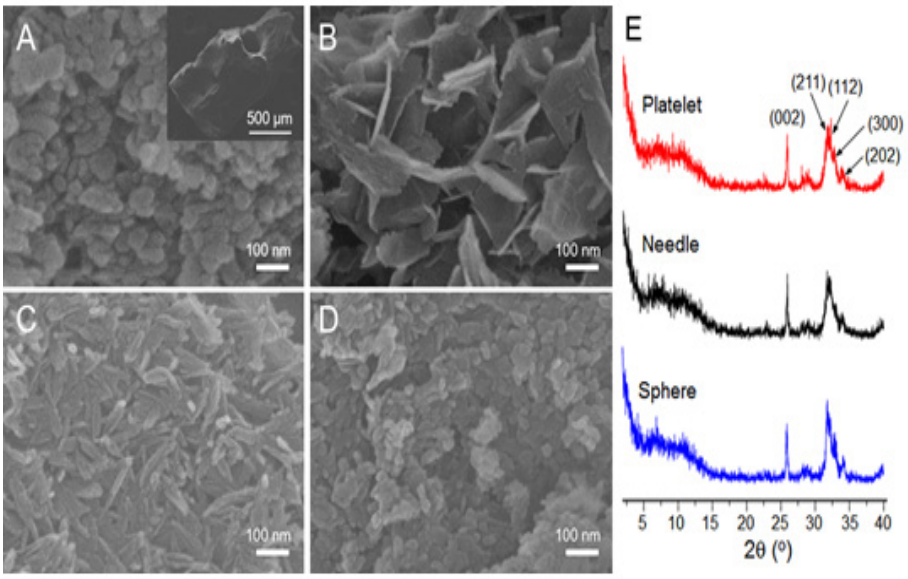

Figure 1: SEM images of the (A) bone graft material (GMs) and (B-D) platelet, needle, and sphere shaped HPs used in the experiments. (E) XRD patterns obtained from HPs with different shapes.

To chemically conjugate HPs on the surface of GMs, we used EDAC and s-NHS chemistries after introducing carboxyl groups on the surface of the GMs and amine groups on the surface of the HPs (see Figure 2 for the scheme of the reaction). Amine groups were attached on the surface of HPs by treating them with AGW®. The attachment of the amine group on the surface of the HPs could be confirmed by FT-IR: two amine stretching peaks and a bending peak were observed at 3100-3700 cm^{-1} and 1753 cm^{-1}, respectively (Figure 3A) [46]. We could also prove the attachment of the amine group on the HP surface by the variation in zeta (ζ) potential (Table 1). The ζ-potential of HPs increased from -22.0 to 4.1 after positive amine groups were functionalized on the NP surface.

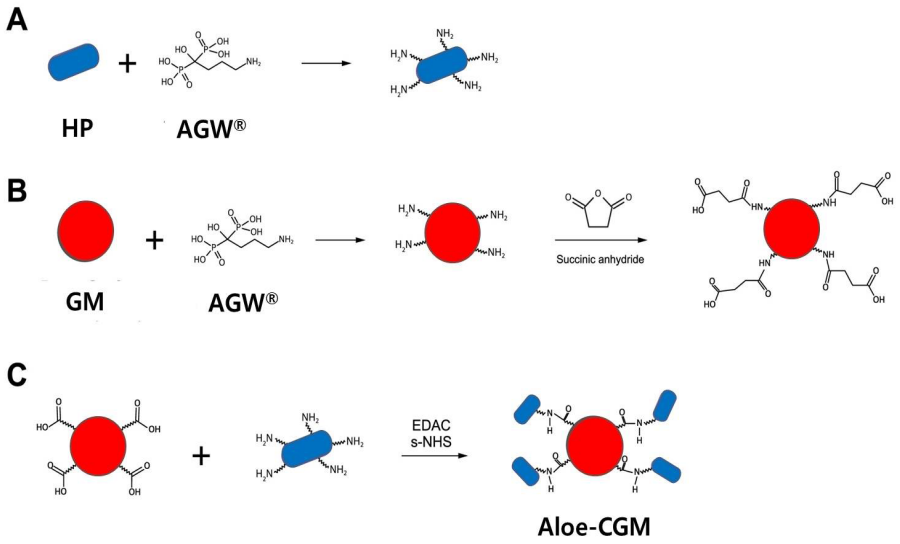

Figure 2: Surface functionalization of (A) HPs and (B) graft materials (GMs) for formation of (C) HP functionalized cuttlefish bone graft materials (Aloe-CGMs).

Carboxyl groups were attached on the surface of the GMs, by sequential treatments of the materials with AGW® and succinic anhydride. The existence of the carboxyl group on the conjugated bone surface could be demonstrated by FT-IR, with a O-H bending peak, a C-O stretching peak, a C=O stretching peak and a O-H stretching peak observed at 920, 1198, 1701, and 2898 cm^{-1}, respectively (Figure 3B) [47].

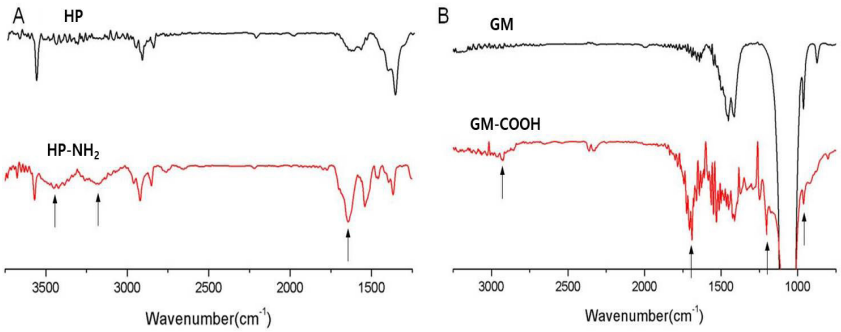

Figure 3: FT-IR spectra of (A) HPs and (B) GMs before and after surface functionalization.

The sequential conjugation process on GMs could also be monitored by the variation in the ζ potential of the material as well (Table 1). After the initial treatment of GMs with AGW®, the ζ potential increased from +0.1 to +10.5 because of the positively charged amine groups on the GMs surface. After the introduction of succinic anhydride to the amine-modified graft materials, we observed the ζ-potential of the graft materials changing to a negative value, from +10.5 to -10.1, because the positively charged amine groups were replaced with negatively charged carboxyl groups. The results of the FT-IR and ζ-potential experiments both demonstrated that carboxylate groups were present on the surface of the graft materials.

Table 1: Zeta-potential variation of GM and HP before and after surface functionalization.

Sample	ζ-potential
HP	-22.0±0.7
HP-NH^2	4.1±0.5
GM	0.2±0.3
GM-NH^2	10.5±0.5
GM-COOH	-10.8±0.7

The chemical reaction between amine groups on HPs and carboxyl groups on the GMs produced GMs with HP surface treatment. The surface morphologies of platelet, needle, and sphere particle-treated GMs are shown in Figure 4. GMs typically had sub 100 nm spherical grains on their surface (see Figure 1A for the SEM image). When platelet shaped HPs were attached on the surface of the GM to form Aloe-CGM with platelet particle treatment (platelet Aloe-CGM), the spherical grains of the graft materials and the platelet shaped HPs were both observed on the surface of the complex structure (see Figure 4A). It is possible that the particle attachment on the graft materials can be made through the electrostatic interaction between the negatively charged carboxylate and positively charged amine modified species rather than covalent conjugation. To prove whether the attachment of the HP on Aloe-CGM was made through covalent binding, we carried out a control experiment, running a parallel conjugation experiment but without both EDAC and s-NHS. When amine-modified platelet shaped HPs and carboxylate GMs were mixed in the absence of EDAC and s-NHS, particles were not observed on the material surface. This verified that the platelet shaped HPs attached on the surface of the GMs were conjugated through covalent attachment. To prepare Aloe-CGMs with needle shaped particle treatment (needle Aloe-CGMs), we went through an identical conjugation process but with needle shaped HPs instead of platelet shaped particles. Through SEM analysis, we could observe both spherical grains of the graft material and needle shaped HPs on the surface of Aloe-CGMs (see Figure 4B). This indicates that needle shaped HPs can be attached on the surface of GMs as well and this chemical conjugation method is not restricted by the morphology of the particles. To obtain Aloe-CGMs with spherical particle treatment (sphere Aloe-CGMs), we attached spherical HPs on the graft materials using the same process. Because both the morphology and approximate size of the spherical particles and the grains of the graft materials were similar, it was impossible to distinguish the particles and grains from the SEM image of the Aloe-CGMs (see Figure 4C). However, we expect a similar amount of sphere shaped HPs attached on the sphere Aloe-CGMs surface to that observed with platelet Aloe-CGMs and needle HPs. To investigate whether the HP attachment on GMs surface can increase its surface area, we carried out BET analysis (see Table 2). GM with no HP attached had a BET surface area of 63.1 m2/g. The three types of Aloe-CGMs samples showed increased surface areas, regardless of the shape of the particles. These data indicate that HPs attached on the surface of graft materials can contribute to increasing its surface area. Among the three HPs attached on the Aloe-CGMs surface, platelet HPs increased the surface area of the GMs most significantly. The surface area of platelet Aloe-CGMs was 92.8 m^2/g, 62.3% higher than GMs with no HP attachment. The needle Aloe-CGMs sample had a surface area of 80.3 m^2/g, a 30.2% increase compared with the control. Sphere Aloe-CGMs had the smallest change, with a surface area of 68.5 m^2/, a 5.2% increase compared with GMs with no HP attachment

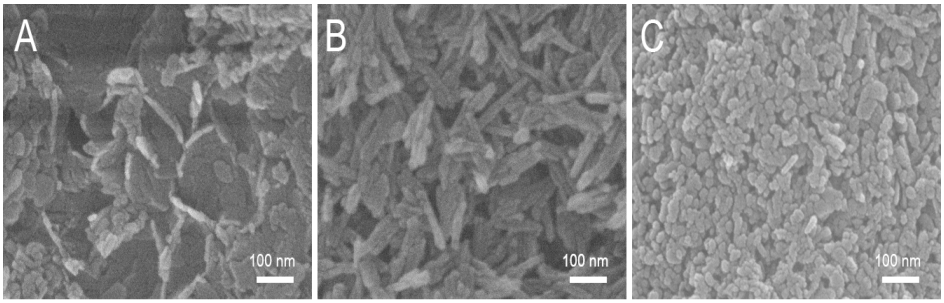

Figure 4: Surface morphology of Aloe-CGMs with (A) platelet, (B) needle, and (C) sphere shaped HPs attached on the surface. On the surface of Aloe-CGMs with platelet and needle particle attachment, both spherical grains and HPs were observed. The platelet and needle shaped particles are in blue for clarification.

Table 2: BET surface areas of GM and platelet, needle, and sphere shaped HP functionalized Aloe-CGMs.

Sample	BET surface area (m^2/g)
GM	63.1
Platelet Aloe-CGM	92.5
Needle Aloe-CGM	80.3
Sphere Aloe-CGM	68.5

As mentioned previously, the average size of the platelet particle (149×72×16 nm) was larger than that of the spherical grains of the graft material (~79 nm). Thus, once the platelet particle binds to the GMs surface, a significant proportion of both platelet particle and graft material surface will still be exposed, with increased surface area and roughness (Figure 5A). The effect of needle shaped HPs on the Aloe-CGMs surface roughness seemed to be smaller than that of platelet particles because needle shaped particles were smaller than platelet particles and their linear structure tends to make them lie down on the surface (Figure 5B). On the other hand, as both the size and shape of the spherical particles were similar to those of the grains of GM, their effect was expected to be somewhat limited.

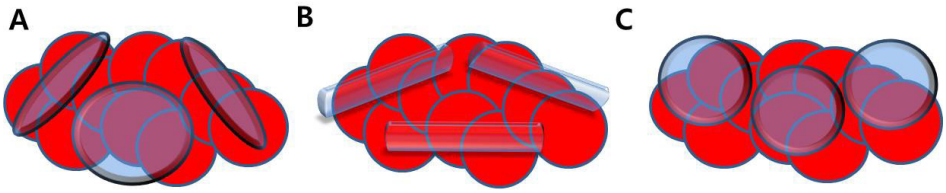

Figure 5: Predicted surface structures of Aloe-CGMs functionalized with (A) platelet, (B) needle, and (C) sphere shaped HPs. The grains of GMs and HPs are colored red and blue, respectively.

Cell Adhesion On Cuttlefish Bone Graft Material

To investigate the number of cells attached to Aloe-CGMs, we cultured MC3T3-E1 cells on the graft material samples and quantified double-stranded DNA extracted from each samples by carrying out a PicoGreen assay (Figure 6). When compared with GM with no particle attachment, all of the Aloe-CGMs had increased activities, regardless of the shape of the HPs attached on the surface. This suggests that HPs attached on the GM surface help to improve its biological activity. Among the three different HPs, platelet shaped particles increased the activity of the graft material most significantly. Compared with the GM, platelet Aloe-CGMs showed approximately 58.8% higher activity ($p<0.002$), while needle Aloe-CGMs showed 25.7% improvements ($p< 0.03$). On the other hand, sphere Aloe-CGMs did not show significant improvement compared to GM. This indicates that two dimensional platelet HP attachment helps cells to bind to the graft materials more efficiently than the one dimensional needle shaped HPs ($p<0.01$) while sphere Aloe-CGMs make insignificant difference.

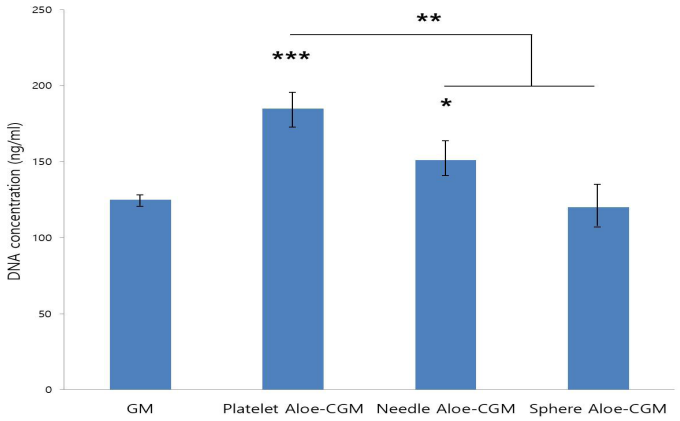

Figure 6: PicoGreen assay data taken from GMs and Aloe-CGMs with different HP attachment. Platelet Aloe-CGMs and needle Aloe-CGMs showed approximately 58.8% ($p<0.002$) and 25.7% ($p<0.03$) improvements compared to GM. On the other hand, sphere Aloe-CGMs did not show significant improvement compared to GM. (*$p<0.03$, **$p<0.01$, ***$p<0.002$).

We consider that cell attachment and proliferation on Aloe-CGMs is closely related to the surface properties of the Aloe-CGMs surface. As mentioned previously, the platelet Aloe-CGM had highest surface area, of 92.3 m^2/g, which was 50.2% higher than GM. Also as large planar particles are attached on small spherical grains of GM, platelet particles can generate porous 3D structures on the surface of platelet Aloe-CGM. So, platelet Aloe-CGMs can work as a scaffold that provides an ideal environment for osteoblasts to bind and grow. Needle shaped HPs also help to increase the surface area of the GMs surface and provide 3D structures on it. However, the biological activities of needle Aloe-CGMs were not as good as platelet shaped HPs. Although needle shaped HPs (120±3 nm) and platelet particles (151±27 nm) had similar long axis lengths, we believe the two dimensional platelet particles were more effective than one dimensional needle shaped HPs in forming surface structures for osteoblasts to bind and proliferate. However, the spherical HPs showed the smallest increase in biological activity, probably because the size and shape of the attached HPs were similar to the spherical grains.

We carried out MTT assay after culturing MC3T3-E1 cells on the synthesized Aloe-CGMs for 24 h to test the cytotoxicity of the synthesized Aloe-CGMs (Figure 7). From the assay, we observed that the viability on the all three types of Aloe-CGMs was similar to GM, regardless of the shape of HPs attached on the Aloe-CGMs surface. This indicates that all three HPs attached on the Aloe-CGMs surface had negligible influence on osteoblast cell viability.

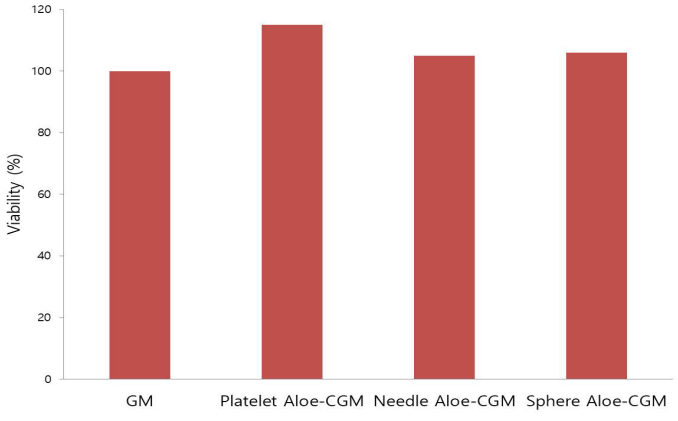

Figure 7: Cell viability determined with the MTT assay from GMs and Aloe-CGMs after 24 h of MC3T3-E1 cell culture.

Conclusion

In summary, we demonstrated a method to improve the biological activity of cuttlefish bone graft materials by chemically AGW® attaching HPs with different shapes on the material surface. Using EDAC-NHS chemistry, we could attach platelet, needle, and sphere shaped HPs on the surface of cuttlefish bone graft materials to form Aloe-CGMs with different surface morphologies. Among the three Aloe-CGMs, the one with platelet HPs attached had the highest biological activity. The platelet Aloe-CGMs improved cell attachment and proliferation of bone graft material ~58.8% and showed negligible cytotoxicity. From these results, we were able to confirm the possibility of clinical entry later.

Acknowledgment

This research was supported by the project entitled 'Technology Development of Marine Industrial Biomaterials' funded by the Korea Institute of Marine Science & Technology Promotion (Program number: 20100090-8).

References

1. Brydone AS, Meek D, Maclaine S (2010) Bone grafting, orthopaedic biomaterials, and the clinical need for bone engineering. Proc Inst Mech Eng Part H-J Eng Med 224(H12):1329-1343. Karageorgiou V, Kaplan D (2005) Porosity of 3D biomaterial scaffolds and osteogenesis. Biomaterials 26(27):5474-5491.
2. Sopyan I, Mel M, Ramesh S, Khalid KA (2007) Porous hydroxyapatite for artificial bone applications. Sci Tech Adv Mater 8(1-2):116-123.
3. Bauer TW, Muschler GF (2000) Bone graft materials-An overview of the basic science. Clin Orthop Relat Res 371:10-27.
4. Eppley BL (1999) Alloplastic implantation. Plast Reconstr Surg 104(6):1761-1783.
5. Al-Asfour A, Andersson L, Kamal M, Joseph B (2013) New bone formation around xenogenic dentin grafts to rabbit tibia marrow. Dent Traumatol 29(6):455-460.
6. Hillier ML, Bell LS (2007) Differentiating human bone from animal bone: A review of histological methods. J Forensic Sci

52(2):249-263.
7. Auchincloss H, Sachs DH (1998) Xenogeneic transplantation. Annu Rev Immunol 16:433-470.
8. Revell CM, Athanasiou KA (2009) Success Rates and Immunologic Responses of Autogenic, Allogenic, and Xenogenic Treatments to Repair Articular Cartilage Defects. Tissue Eng Part B Rev 15(1):1-15.
9. Yildirim M, Spiekermann H, Biesterfeld S, Edelhoff D (2000) Maxillary sinus augmentation using xenogenic bone substitute material Bio-Oss (R) in combination with venous blood-A histologic and histomorphometric study in humans. Clin Oral Implants Res 11(3):217-229.
10. Venkatesan J, Rekha PD, Anil S, Bhatnagar I, Sudha PN, Dechsakulwatana C, Kim SK, Shim MS (2018) Hydroxyapatite from cuttlefish bone: isolation, characterizations, and applications. Biotechnology Bioprocess Engineering 23(4):383-393.
11. Kieswetter K, Schwartz Z, Dean DD, Boyan BD (1996) The role of implant surface characteristics in the healing of bone. Crit Rev Oral Biol Med 7(4):329-345.
12. Korovessis PG, Deligianni DD, Lenke LG (2002) Role of surface roughness of titanium versus hydroxyapatite on human bone marrow cells response. J Spinal Disord Tech 15(2):175-183.
13. Tabassum A, Walboomers F, Wolke JGC, Meijer GJ, Jansen JA (2011) The Influence of Surface Roughness on the Displacement of Osteogenic Bone Particles during Placement of Titanium Screw-Type Implants. Clin Implant Dent Relat Res 13(4):269-278.
14. Segal E, Perelman LA, Cunin F, Di Renzo F, Devoisselle J-M, Li YY, MJ Sailor (2007) Confinement of thermoresponsive hydrogels in nanostructured porous silicon dioxide templates. Adv Funct Mater 17(7):1153-1162.
15. Ooi CY, Hamdi M, Ramesh S (2007) Properties of hydroxyapatite produced by annealing of bovine bone. Ceram Int 33(7):1171-1177.
16. Wei GB, Ma PX (2004) Structure and properties of nano-hydroxyapatite/polymer composite scaffolds for bone tissue engineering. Biomaterials 25(19):4749-4757.
17. Guo X, Gough JE, Xiao P, Liu J, Shen Z (2007) Fabrication of nanostructured hydroxyapatite and analysis of human osteoblastic cellular response. J Biomed Mater Res Part A 82A(4):1022-1032.
18. Meskinfam M, Sadjadi MA, Jazdarreh H, Zare K (2011) Biocompatibility Evaluation of Nano Hydroxyapatite-Starch Biocomposites. J Biomed Nanotechnol 7(3):455-459.
19. Henkel K-O, Gerber T, Lenz S, Gundlach KKH, causa h, Bienengraeber V (2006) Macroscopical, histological, and morphometric studies of porous bone-replacement materials in minipigs 8 months after implantation. Oral Surg Oral Med Oral Pathol Oral Radiol Endod 102(5):606-613.
20. Suchanek W, Yoshimura M (1998) Processing and properties of hydroxyapatite-based biomaterials for use as hard tissue replacement implants. J Mater Res 13(1):94-117.
21. Mostafa NY (2005) Characterization, thermal stability and sintering of hydroxyapatite powders prepared by different routes. Mater Chem Phys 94(2-3):333-341.
22. Kim HW, Song JH, Kim HE (2005) Nanoriber generation of gelatin-hydroxyapatite biomimetics for guided tissue regeneration. Adv Funct Mater 15(12):1988-1994.
23. Hong Z, Zhang P, He C, Qiu X, Liu A, et al. (2005) Nano-composite of poly(L-lactide) and surface grafted hydroxyapatite: Mechanical properties and biocompatibility. Biomaterials 26(32):6296-6304.
24. Wang YW, Wu Q, Chen J, Chen GQ (2005) Evaluation of three-dimensional scaffolds made of blends of hydroxyapatite and poly(3-hydroxybutyrate-co-3-hydroxyhexanoate) for bone reconstruction. Biomaterials 26(8):899-904.
25. Kaito T, Myoui A, Takaoka K, Saito N, Nishikawa M, et al. (2005) Potentiation of the activity of bone morphogenetic protein-2 in bone regeneration by a PLA-PEG/hydroxyapatite composite. Biomaterials 26(1):73-79.
26. Yu S, Hariram KP, Kumar R, Cheang P, Aik KK (2005) In vitro apatite formation and its growth kinetics on hydroxyapatite/polyetheretherketone biocomposites. Biomaterials 26(15):2343-2352.
27. Kong L, Gao Y, Cao W, Gong Y, Zhao N, Zhang X (2005) Preparation and characterization of nano-hydroxyapatite/chitosan composite scaffolds. J Biomed Mater Res Part A 75A(2), 275-282.
28. Tachibana A, Kaneko S, Tanabe T, Yamauchi K (2005) Rapid fabrication of keratin-hydroxyapatite hybrid sponges toward osteoblast cultivation and differentiation. Biomaterials 26(3):297-302.
29. Shalumon KT, Sowmya S, Sathish D, Chennazhi KP, Nair Shantikumar V, et al. (2013) Effect of Incorporation of Nanoscale Bioactive Glass and Hydroxyapatite in PCL/Chitosan Nanofibers for Bone and Periodontal Tissue Engineering. J Biomed Nanotechnol 9(3):430-440.
30. Rauschmann MA, Wichelhaus TA, Stirnal V, Dingeldein E, Zichner L, et al. (2005) Nanocrystalline hydroxyapatite and calcium sulphate as biodegradable composite carrier material for local delivery of antibiotics in bone infections. Biomaterials 26(15):2677-2684.
31. Cheng K, Weng W, Wang H, Zhang S (2005) In vitro behavior of osteoblast-like cells on fluoridated hydroxyapatite coatings. Biomaterials 26(32):6288-6295.
32. Kim HW, Kim HE, Salih V, Knowles JC (2005) Sol-gel-modified titanium with hydroxyapatite thin films and effect on osteoblast-like cell responses. J Biomed Mater Res Part A 74A(3):294-305.
33. Cyster LA, Grant DM, Howdle SM, Rose FR, Irvine DJ, et al. (2005) The influence of dispersant concentration on the pore morphology of hydroxyapatite ceramics for bone tissue engineering. Biomaterials 26(7):697-702.
34. Shikinami Y, Okuno M (1999) Bioresorbable devices made of forged composites of hydroxyapatite (HA) particles and poly-L-lactide (PLLA): Part I. Basic characteristics. Biomaterials 20(9):859-877.
35. Zhang R, Ma PX (1999) Poly(alpha-hydroxyl acids) hydroxyapatite porous composites for bone-tissue engineering. I. Preparation and morphology. J Biomed Mater Res 44(4):446-455.
36. Han GS, Lee S, Kim DW, Kim DH, Noh JH, et al. (2013) A Simple Method To Control Morphology of Hydroxyapatite Nano and Microcrystals by Altering Phase Transition Route. Cryst Growth Des 13(8):3414-3418.
37. Zhuang Z, Yamamoto H, Aizawa M (2012) Synthesis of plate-shaped hydroxyapatite via an enzyme reaction of urea with urease and its characterization. Powder Technol 222:193-200.

38. Kim DM, Kim HJ, Kang HC, Ahn HC, Kim YM, et al. (2014) Comparison of bone repair treated with Balanus glandula cement, *Aloe vera* gel (AGW®) nanofibrous cuttlefish graft in rat calvaria. J Biomed Eng Res 58(2):58-66.
39. Kim DM, Lee HK, Kwon YS, Choi YM (2022) Enhanced bone regeneration by *Aloe vera* gel (AGW®) conjugated barnacle cement protein composite hyaluronic acid hydrogel based hydroxyapatite derived from cuttlefish bone. Medical Clinical Research 7(3):1-9.
40. Schuessele A, Mayr H, Tessmar J, Goepferich A (2009) Enhanced bone morphogenetic protein-2 performance on hydroxyapatite ceramic surfaces. J Biomed Mater Res Part A 90A(4):959-971.
41. Lee HJ, Nguyen YT, Muthiah M, Vu-Quang H, Namgung R, et al. (2012) MR traceable delivery of p53 tumor suppressor gene by PEI-functionalized superparamagnetic iron oxide nanoparticles. J Biomed Nanotechnol 8(3):361-371.
42. Shu R, McMullen R, Baumann MJ, McCabe LR (2003) Hydroxyapatite accelerates differentiation and suppresses growth of MC3T3-E1 osteoblasts. J Biomed Mater Res Part A 67A(4):1196-1204.
43. Viswanath B, Ravishankar N (2008) Controlled synthesis of plate-shaped hydroxyapatite and implications for the morphology of the apatite phase in bone. Biomaterials 29(36):4855-4863.
44. Milev A, Kannangara GSK, Ben-Nissan B (2003) Morphological stability of hydroxyapatite precursor. Mater Lett 57(13-14):1960-1965.
45. Kim YK, Suh SY, Romij MD, Kim YB, Kim HH, et al. (2013) Variation in amino acid content among three Aloe Species. Asian Journal of Chemistry 25(11):6346-6348.
46. Karina DIS, Antonio VG, Kong AH, Yissleen NM, Gipsy TM, et al. (2013) Chemical and physical properties of *Aloe vera* (*Aloe barbadensis* Miller) gel stored after high hydrostatic pressure processing. Food Sci Technol 33(1):52-59.